A98-31511 ICAS-98-2,6,2

PROPELLER SLIPSTREAM COMPUTATIONAL METHODS

D. Wang, P. Eliasson, S. Meijer and I. Lindblad
The Aeronautical Research Institute of Sweden, FFA
P.O. Box 11021, S-161 11 Bromma
Sweden

Abstract

The paper presents unsteady Euler computations through non-matching and sliding-zone interface for three-dimensional problems. An interpolation scheme together with an efficient search algorithm is used at the interface to find the interpolation weights. The accuracy of the approach will be demonstrated numerically by propeller results at typical cruise conditions for a propeller driven aircraft. Slipstream field analysis of a propeller-wing combination will be presented in the paper.

The potential of using the actuator disc model as an alternative to detailed time accurate propeller calculations will be discussed.

The investigation reveals the propeller slipstream features and the character of different propeller computational methods.

Summary

For a propeller driven aircraft it is crucial to be able to predict, control and reduce the cabin noise induced from the propeller. The propeller time dependent slipstream may considerably affect the flow over the nacelle, wing and stabilizer. The prediction of these effects is important in the design process. It is highly desirable to be able to directly calculate the unsteady field of propeller driven aircraft. Due to the increased computer capacity, Euler and Navier-Stokes codes have become increasingly affordable for unsteady CFD.

In order to investigate the validity of simplified propeller models it is valuable to study how results from such models are related to results from detailed time accurate propeller calculations.

The computation over an aircraft with a rotating propeller requires an interface between the stationary and rotating part of the computational domain. The feasibility of using patched sliding-zone interfaces has been demonstrated previously for time accurate rotor stator interactions. Earlier investigations also have been made for the effects of a patched sliding-zone interface on the transmission of acoustic waves, but the interpolation was restricted to topologically equivalent interfaces.

A completely general patched sliding zone interface approach without restriction on mesh topology for three-dimensional problems is adopted in our code. An efficient search algorithm has been constructed in the code to find the interpolation weights and a bilinear interpolation is carried out for the primitive variables. The transmission of a 3D acoustic wave propagating throuth thé interface (either matching, non-matching or sliding) in a duct has been investigated with respect to accuracy in space and time. A new efficient scheme for time accurate Euler and Navier-Stokes predictions is used.

In the present paper the accuracy of the approach will be demonstrated numerically for a 4-blade propeller by comparing results from the time accurate calculations with results from calculations performed in a rotating frame of reference. Results of calulations for a 4-blade propeller with a wing behind will be presented. Earlier work in propeller modeling will be cited and the potential of using the actuator disc model as an alternative to detailed time accurate propeller calculations will be discussed.

Methodology

Description of the Computer Code

The flow solver EURANUS [1] is used. The solver solves the 3D time-dependent Navier-Stokes equations in a cell centered finite volume formulation for structured multi-block grid. The blocks can be connected in a one-to-one manner or patched non-matching without restriction on the connected grid topology. The steady state part of the code is explicit in time with local time steps, implicit residual smoothing and mutigrid to accelerate the convergence.

EURANUS can also be used for time accurate computations with explicit Runge-Kutta time marching or, for most practical applications, implicit time integration with pseudo time relaxation[2][3][4]. Central differences with artificial dissipation, upwind symmetric TVD or flux difference TVD are the spatial discretizations available. Viscous terms, when present, are centrally differenced.

The code offers equilibrium and non-equilibrium

for reacting gases, a number of turbulence models, parallelization using PVM etc.

Numerical Method

In this paper only the Euler equations are considered. The compressible Euler Equations can be expressed as

$$\frac{\partial}{\partial t}q + \nabla \cdot F = 0 \qquad (1)$$

where q contains the conservative variables and F is flux tensor

$$q = \begin{pmatrix} \rho \\ \rho u \\ \rho v \\ \rho w \\ e \end{pmatrix}, F = \begin{pmatrix} \rho u & \rho v & \rho w \\ \rho uu & \rho vu & \rho wu \\ \rho uv & \rho vv & \rho wv \\ \rho uw & \rho vw & \rho ww \\ (e+p)u & (e+p)v & (e+p)w \end{pmatrix}.$$

Differencing in space with a control volume approach is applied. The numerical flux evaluated on the cell faces can lead to either central or upwind scheme. Here we chose a central approach with artificial dissipation. The artificial dissipation is a blending of 2nd and 4th differences of the conservative variables[5].

An implicit approach with pseudo time relaxation[2][3][4] is used to advance the solution in time. A second order backward difference method is employed. The steady state problem is solved with explicit pseudo time marching combined with multigrid, local time steps and implicit residual smoothing.

A patched non-matching interface implies that two blocks share a common boundary or interface at which grid points do not necessarily connect in a one-to-one manner. Interpolation weights must be determined for the variables to allow a time accurate transfer of data between the blocks. For sliding interfaces the interpolation weights have to be recomputed each time step. A completely general patched sliding zone interface approach without restriction on mesh topology for three-dimensional problems is adopted in EURANUS[6]. A sophisticated search algorithm has been constructed in the code to find the interpolation weights and a bilinear interpolation is carried out for the primitive variables[6]. The transmission of a 3D acoustic wave propagating through the interface (either matching, non-matching or sliding) in a duct has been investigated with respect to accuracy in space and time[6]. In the paper, the accuracy of the sliding zone interface approach will be demonstrated numerically in a basic application case. Results from a time accurate calculation for a 4-blade propeller will be compared with results from a steady calculation in a rotating frame of reference.

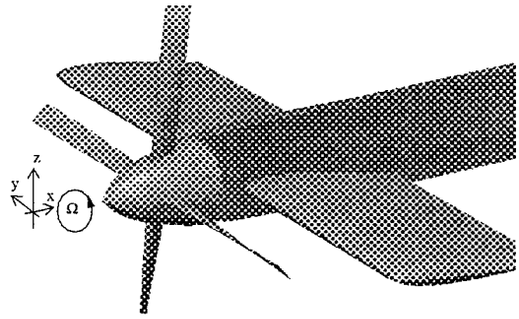

Figure 1: Geometry of the 4-blade propeller with spinner and wing

Numerical Results

A central scheme is used with a minium of dissipation. The time accurate calculations start from steady results. Results are presented during the second period. 192 implicit time steps per period is used. About 30 multigrid cycles per time step is required to reduce the residuals about 3 orders each time step.

Calculation Model

A case representing typical cruise condition for a commercial aircraft, has been chosen to investigate the propeller slipstream field.

The propeller has 4 blades and a radius of $r_p = 1.6m$. The blades are unswept with constant chord $C = 0.2m$. The airfoil sections are of the 4 digit symmetric NACA series. The blade is twisted around the pitch change axis, which is placed at $0.25C$ on the airfoil mean line. The propeller is mounted on an axisymmetric sting. The blades are located from $x = -0.0498$ to $x = 0.1485$, where $x = 0$ corresponds to the position of the pitch change axis.

In the case of wing-propeller combination, we use the same 4 bladed propeller as described above and a wing with constant chord of $1.6m$ and $4.5m$ span is mounted on the spinner behind the propeller. The wing airfoil is NACA0012. The mounted angle of the wing is 6° relative to the x axis and the pitch change axis of the wing is at 25% of the chord on the airfoil mean line. See figure 1 and figure 2

The free stream Mach number $M_\infty = 0.5$ and the incoming flow is in in the x-axis direction, see figure 1. The propeller angular velocity is 124.93067 rad/sec with the direction opposite to the x-axis i.e $\Omega = (-124.93067, 0, 0)$. The tip helical Mach number $M_{hel} = 0.8$.

In the results shown in the paper, the pressure is scaled by the undisturbed static pressure. The velocity components are scaled by the undisturbed velocity value. The circumferential velocity V_{cir} is defined as a positive value when it has the same direction as the propeller rotation direction in the calculation examples. If the coordinates are scaled by the propeller

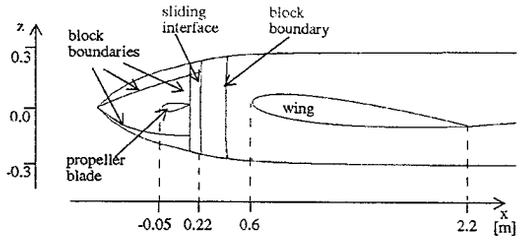

Figure 2: Spinner with mounted propeller and wing and location of the sliding interface

radius it will be pointed out.

Propeller Calculation

The time accurate calculation results for a 4-blade propeller will be compared with results from a steady calculation in a rotating frame of reference [7][8][9] to demonstrate numerically the accuracy of the sliding zone interface approach. The steady calculation for this propeller was well investigated in the respect of space resolution, slipstream development etc.[9].

1. Computational grid The grid is generated with the grid generation tool FFANET[10].

The finest grid for the propeller steady calculations is one block $289 \times 65 \times 65$. It is a C-grid around the blade with 289 nodes and with 97 nodes concentrated on the blade in the chord-wise direction. The C-grid consists of 65 layers stacked on top of one another, 41 stations are placed on the propeller blade along the radial direction. In order to analyze the slipstream in the near field, among the 97 stations behind the blade trailing edge, there are 29 stations concentrated after the blade trailing edge within about one blade chord length. There are 72 stations placed after the blade trailing edge within about 10 times the blade chord length, and 80 stations within the propeller diameter distance. The grid extends a distance of 2.813 times the propeller radius in the upstream and radial direction. In the downstream direction it extends a distance of 3.75 times the propeller radius. The coarse grid of steady calculation in the rotating frame of reference is $145 \times 33 \times 33$, created by taking away every second node in every directions from the grid $289 \times 65 \times 65$.

In the time accurate calculation, The grid is $4 \times 145 \times 33 \times 33$ with 6 blocks. The grid is the same as the coarse grid of steady calculation around each blade. The 4 blade blocks are ended at trailing edges. A rotating block is connected with 4 blade blocks and ended with a sliding interface at $x = 0.4$. For this block the grid is changed gradually from being concentrated on the wake region at the trailing edge to equally distributed in circumferential direction at $x = 0.4$. After the sliding interface there is a steady block with equally distributed grid in circumferential direction. For these two blocks the grids keep the same distribution in x and radial directions as the coarse grid of steady calculation.

2. Calculation results We select three radial lines at $x = 0.15$, $x = 0.35$ and $x = 0.60$ respectively to present the results in order to demonstrate numerically the accuracy of the sliding zone interface approach in the application case. The three positions $x = 0.15$, $x = 0.35$ and $x = 0.60$ are corresponding to the trailing edge x coordinate of the propeller, one chord length downstream of the propeller trailing edge (which is in the rotationg block with sliding interface for time accurate calculations) and the position in the steady block behind the sliding interface for time accurate calculations (This is also the wing leading edge x coordinate in the propeller-wing combination calculation geometry) respectively.

The results shown here are circumferential velocity only on three lines, as other variables have similar character in comparisions. V_{cir} is the circumferential velocity component scaled by free stream velocity value and the line length coordinates are scaled by propeller radius. The results are shown at 8 different times. For each new time the propeller has been rotated 11.25° and thus after 8 time steps the propeller has been rotated 90° which corresponds to one period in time. Using the angle as a subscript the results are shown for times t_0, $t_{11.25}$, $t_{22.5}$, $t_{33.75}$, t_{45}, $t_{56.25}$, $t_{67.5}$ and $t_{78.75}$. The results at t_0, $t_{22.5}$, t_{45}, $t_{67.5}$ are shown on the left side represented by solid line, dashed line, fine dashed line and dot-dashed line respectively in figure 3 and 4. The results at time $t_{11.25}$, $t_{33.75}$, $t_{56.25}$ and $t_{78.75}$ are shown on the right side by solid line, dashed line, fine dashed line and dot-dashed line respectively in figure 3 and 4. The upper figures in figure 3 and 4 are V_{cir} on the radial line at $x = 0.15$. The middle figures are V_{cir} on the radial lines at $x = 0.35$. The lower figures are V_{cir} on the radial line at $x = 0.60$.

The steady calculation results in a rotating frame of reference are shown in figure 3. They are the comparisions between the finer grid and coarser grid at different times. In these figures the results using the coarser grid have sufficient resolution to represent the propeller slipstream field. Therefore the coarser grid is utilized to form a 6 block grid for time accurate computations (through non-matching and sliding-zone interfaces).

The time accurate computation through non-matching and sliding-zone interfaces for the propeller results are shown in figure 4. They are the comparisions between time accurate results and steady calculation results in a rotating frame of reference. The time t_0 is the time when the propeller blades are located at vertical positions (for another two at the horizontal position). At position $x = 0.15$ (upper figure 4), it is hard to see the difference between the two different methods. At $x = 0.35$ (middle figure 4), one can see some deviation at $t_{11.25}$. At $x = 0.60$

(lower figure 4), one can see some deviation at $t_{22.5}$. We should point out that, the deviations mentioned above, is caused by the grid differences in the circumferential distributions and not by the different methods. Because the $t_{11.25}$ for $x = 0.35$ and $t_{22.5}$ for $x = 0.60$ are corresponding to the times when the propeller wake sweep over the lines. At those moments there is a need for a fine grid resolution in circumferential direction to represent the small scale wake in detail, see[9].

Propeller-Wing Combination Calculation Results

1. Computational grid The computational grid has 9 blocks with a possibility of multigrid calculation and is generated by FFANET. The grid around the blades are the same as for the propeller time accurate calculation grid, but the rotating block with sliding interface behind the blade blocks is ended at $x = 0.22$ see figure 2. A C-O topology is chosen around the wing. It is refined around the chord (with 96 cells) and coarsened away from the wing. There are 25 stations in spanwise direction for every part of the wing. Altogether the grid has 0.55 million grid points.

2. Pressure distribution on the wing The pressure distribution and variation in time on the wing can be seen in figure 5 at $y \sim \pm 0.38$ (the wing at root intersection), $y = \pm 0.8$, $y = \pm 1.2$, $y = \pm 1.6$ and $y = \pm 2.0$ (outside of propeller sweep radius) from left to the right respectively.

The pressure distribution reveals that there is larger variation of pressure in time on the right wing where there is an upwash from the propeller which results in a higher angle of attack, see figure 1. This increase in angle of attack is also obvious on the pressure levels. At $y = -2.0$ there is stronger variation with time, and the pressure level is relatively high. The increased suction peaks and increased suction level variation with time towards the spinner surface on the right wing ($y < 0$) can be seen also.

However the pressure distribution on the left wing ($y > 0$) does not change very much with time compared to the right wing. And the pressure level is relatively higher than on the right wing, which is expected because of the influence from the propeller.

The results above indicate that the noise contribution from the part of the wing that experiences an upwash would be higher than from the downwash side. The integrated load of the wing does not strongly vary with time.

In this example, the wing is extremely close to the propeller compared with a real propeller driven aircraft. The distance between wing leading edge and propeller is less than a half wing chord length. And the mounted wing angle is higher. The purpose of selecting this model is to investigate the influence between them. In the paper[6] it was suspected that the difference in time variation of the results from the right and the left side of the wing was due to grid resolution problems. The grid for the right and left are the same, and further investigation has shown that the character on the left wing is reasonable. There is a strong upwash from the wing in this example, it cancels the propeller downwash on the left side behind the propeller. The phenomenon can be explained in the next section.

3. Slipstream field study We select two x positions to show the slipstream field. One position is $x \sim 0.15$, the propeller trailing edge grid surface. And another is $x = 0.22$ grid surface, which is the sliding surface located in front of the wing. For these two positions, the grid is almost the same as for the propeller alone calculation. The grid resolution was sufficient for the propeller alone case. Behind $x = 0.22$ there is coarser (but not corser in x direction) grid for the propeller-wing combination.

In figure 6 are the V_{cir} fields on the $x = 0.22$ grid surface at t_0, $t_{22.5}$, t_{45} and $t_{67.5}$ respectively. The subscript for t represent how many degree the blades has been rotated from vertical position (or horizontal position). It is obvious that in front of the wing there is strong variation with time on right side and a slight variation with time on the left.

In figure 7 are the V_{cir} fields on the $x \sim 0.15$ grid surface at t_0, $t_{22.5}$, t_{45} and $t_{67.5}$ respectively. If we compare these figures with propeller alone on the $x \sim 0.15$ grid surface figure 8, they are quite close to each other. The influence from the wing changes the periodic character in circumference-wise, but the V_{cir} values are about the same.

From these figures, we may explain the results on figure 5 for the left wing. Obviously no matter how strong the influence from the wing, the field at the blade trailing edge position is still dominated by the propeller. Less than half chord of the blade downstream the field has a strong influence from the wing in the example.

Potential of Using Actuator Disc Models

We have investigated the propeller disc models in Euler Equations[7][8][9]. The calculation model is the same propeller geometry at $M_\infty = 0.5$ and $M_{hel} = 0.8$ mentioned above.

From the propeller-wing combination time accurate calculation results we have noticed that:

- The integrated load of the wing does not strongly vary with time.
- No matter how strong influence from wing, the field at blade trailing edge position is still dominated by the propeller. Less than half chord of the blade downstream the field has strong influence from the wing in the example.

This support the use of the time-averaged disc model in the engineering applications. Though in the steady calculations the disc data will not be adjusted by the influence of wing, not far downstream the flow field will be adjusted.

In the paper[9], validation of disc model is presented. The comparison between the time averaged results of propeller calculations and the results of the time-averaged disc model calculations can be seen in figures 9 to 12. The time-averaged disc force data is generated by the steady calculation (in a rotating frame of reference) of the propeller results. The results of the propeller are time averaged (azimuthally averaged in a rotating system). In all of the figures, the abscissa is x/r_p and the ordinate is r/r_p, the left figures for the time averaged results of the propeller calculations, and the right figures for the results of time-averaged disc model calculations. Figures 9 to 12 show the static pressure, circumferential velocity, radial velocity and the axial velocity fields, respectively. The agreement between the time averaged results of datailed propeller calculations and the results of the time-averaged disc model calculations is good in the whole field. This can be explained by the propeller field character[9].

Conclusions

The unsteady computations through non-matching and sliding-zone patched interface is used for three-dimensional problems. The accuracy of the sliding zoon interface approach have been demonstrated numerically in a basic application case, a 4-blade propeller with time accurate results. The computations for the propeller and propeller-wing combination show satisfactory results and demonstrates the feasibility of the method. And also it convinces of the potential for using the actuator disc model as an alternative to full detailed propeller calculations in the engineering applications.

References

[1] A. Rizzi, P. Eliasson, I. Lindblad, , C. Hirsch, C. Lacor and S. Häuser, 1993, The Engineering of Multiblock/Multigrid Software for Navier-Stokes Flows on Structured Meshes, Computers & Fluids, vol. 22, pp. 341-367.

[2] A. Jameson, 1991 Time Dependent Calculations using Multigrid, with Applications to Unsteady Flows past Airfoils and Wings, AIAA 91-1596.

[3] P. Eliasson and J. Nordström, 1995, The Development of an Unsteady Solver for Moving Meshes, FFA TN 1995-39

[4] P. Eliasson, J. Nordström, L. Torngren, L. Tysell, A. Karlsson, B. Winzell, 1996, Computations and Measurements of Unsteady Pressure on a Delta Wing with an Oscillating Flap, Proc. of 3rd ECCOMAS CFD Conf., pp.478-484.

[5] A. Jameson, W. Schmidt, E. Turkel, 1981, Numerical Solutions of the Euler Equations by Finite Volume Methods using Runge-Kutta time-Stepping Schemes, AIAA 81-1259.

[6] P. Eliasson, D. Wang, S. Meijer, J. Nordström, 1998, Unsteady Euler Computations through Non-Matching and Sliding-Zoon Interfaces, AIAA-98-0371.

[7] D. Wang, I. Lindblad, P. Eliasson, 1996, Analysis of Propeller Slipstream Field, ICAS-96-4.10.5.

[8] D. Wang, I. Lindblad, 1997, Characters of Propeller Models in Euler Equations, AIAA 97-0402.

[9] D. Wang, I. Lindblad, 1997, Investigation of Propeller Models in Euler Equations, FFA TN 1997-06.

[10] L. Tysell and S. Hedman, 1988, Towards a general three-dimensional grid generation system, ICAS Paper 88-4.7.4.

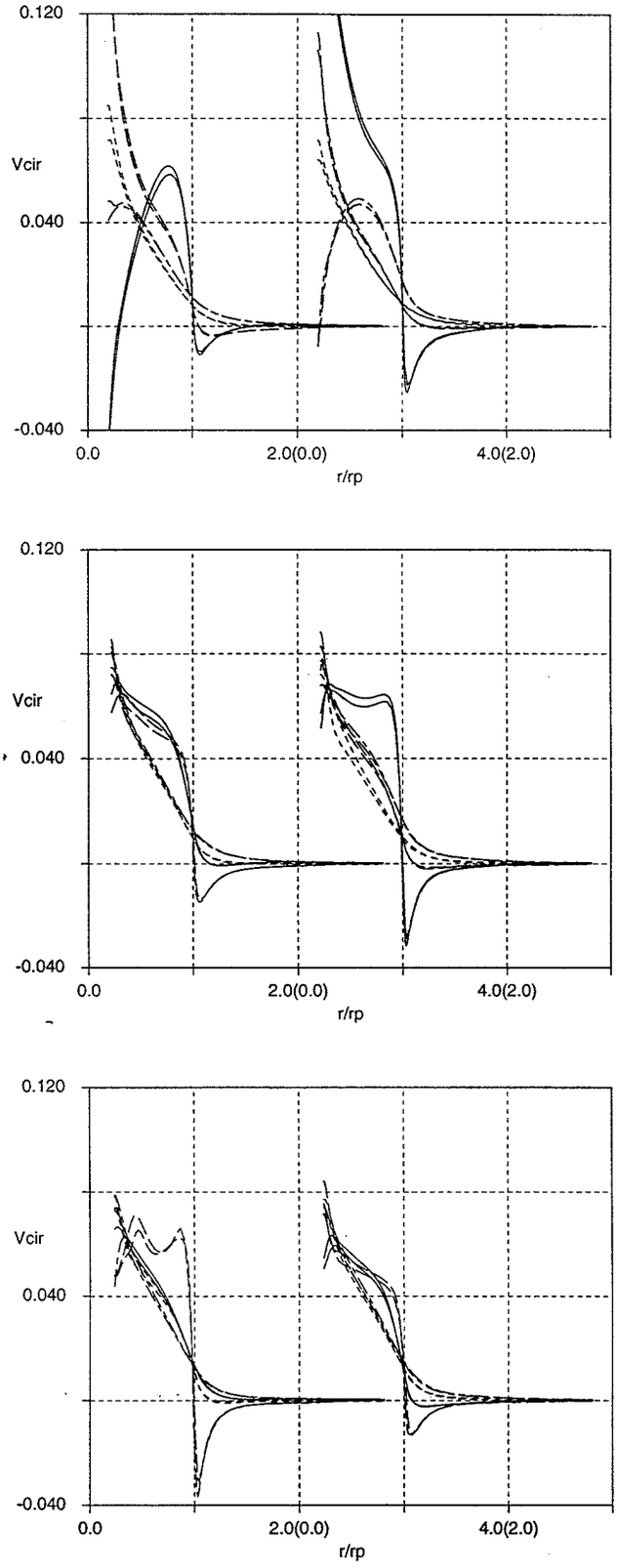

Figure 3: Comparision between finer and coarser grid results in steady calculations V_{cir} on radial lines at $x = 0.15$(upper), $x = 0.35$(middle), $x = 0.60$(lower)

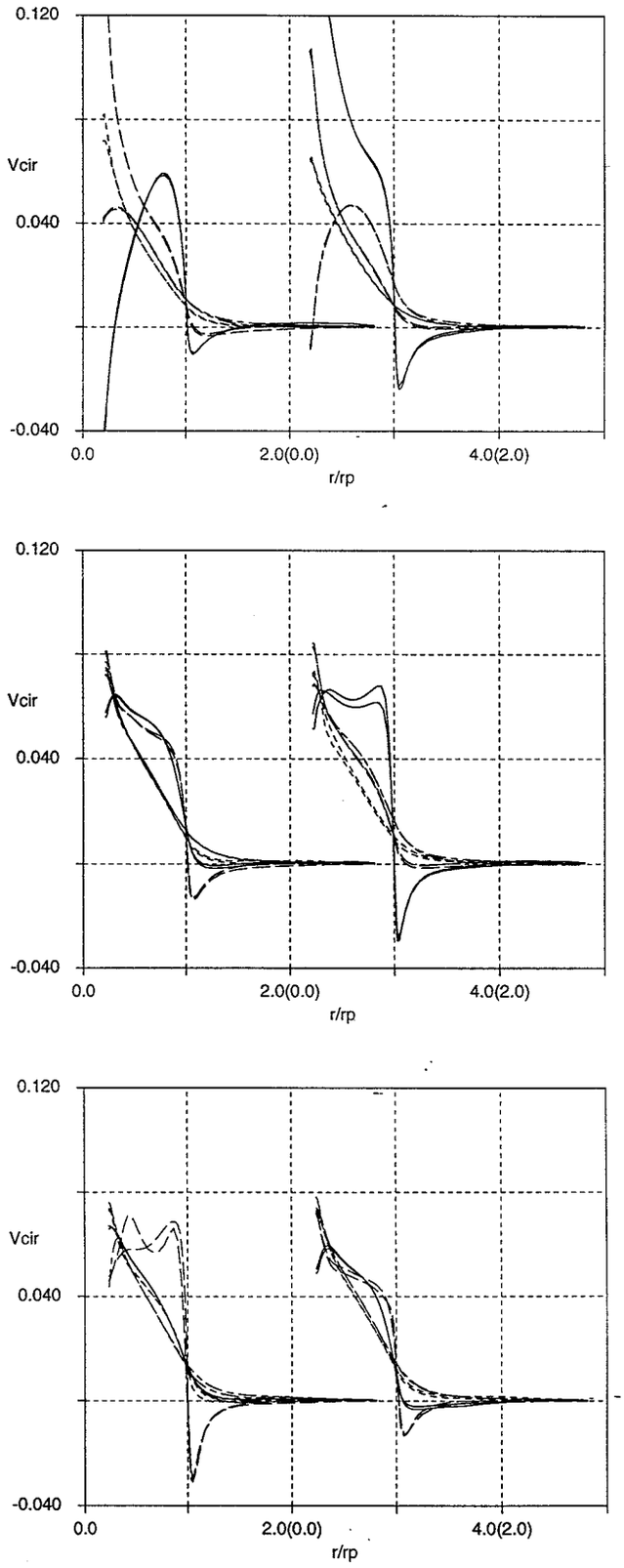

Figure 4: Comparision between time accurate and steady calculation results V_{cir} on radial lines at $x = 0.15$(upper), $x = 0.35$(middle), $x = 0.60$(lower)

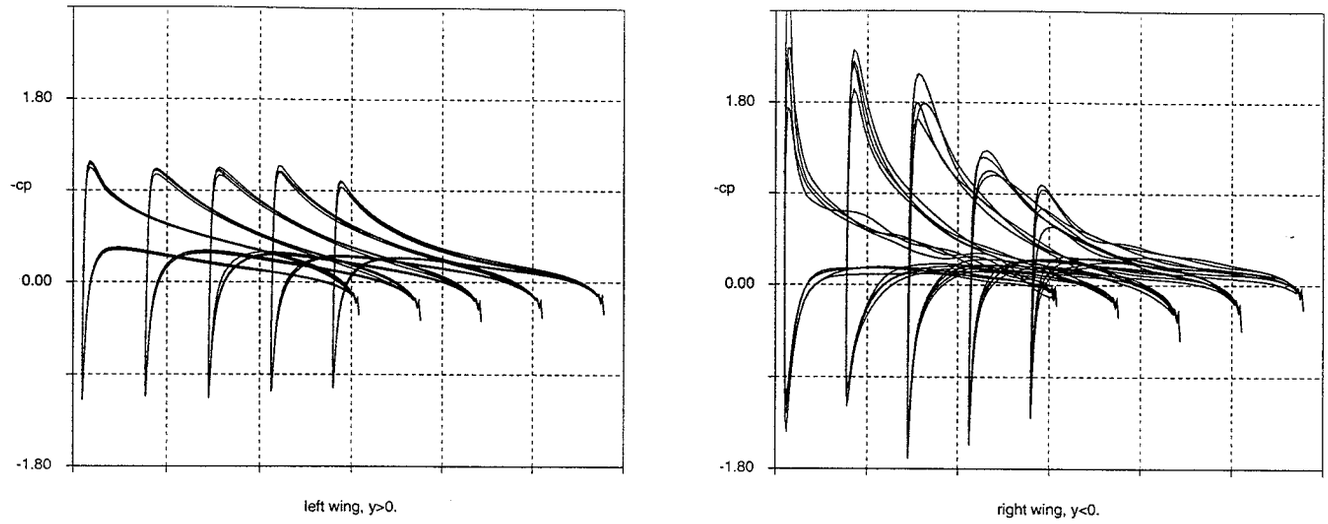

Figure 5: Pressure variation in time on the wing at different span wise positions (from left to right:$y \sim \pm 0.38$,$y = \pm 0.8$,$y = \pm 1.2$,$y = \pm 1.6$,$y = \pm 2.0$)

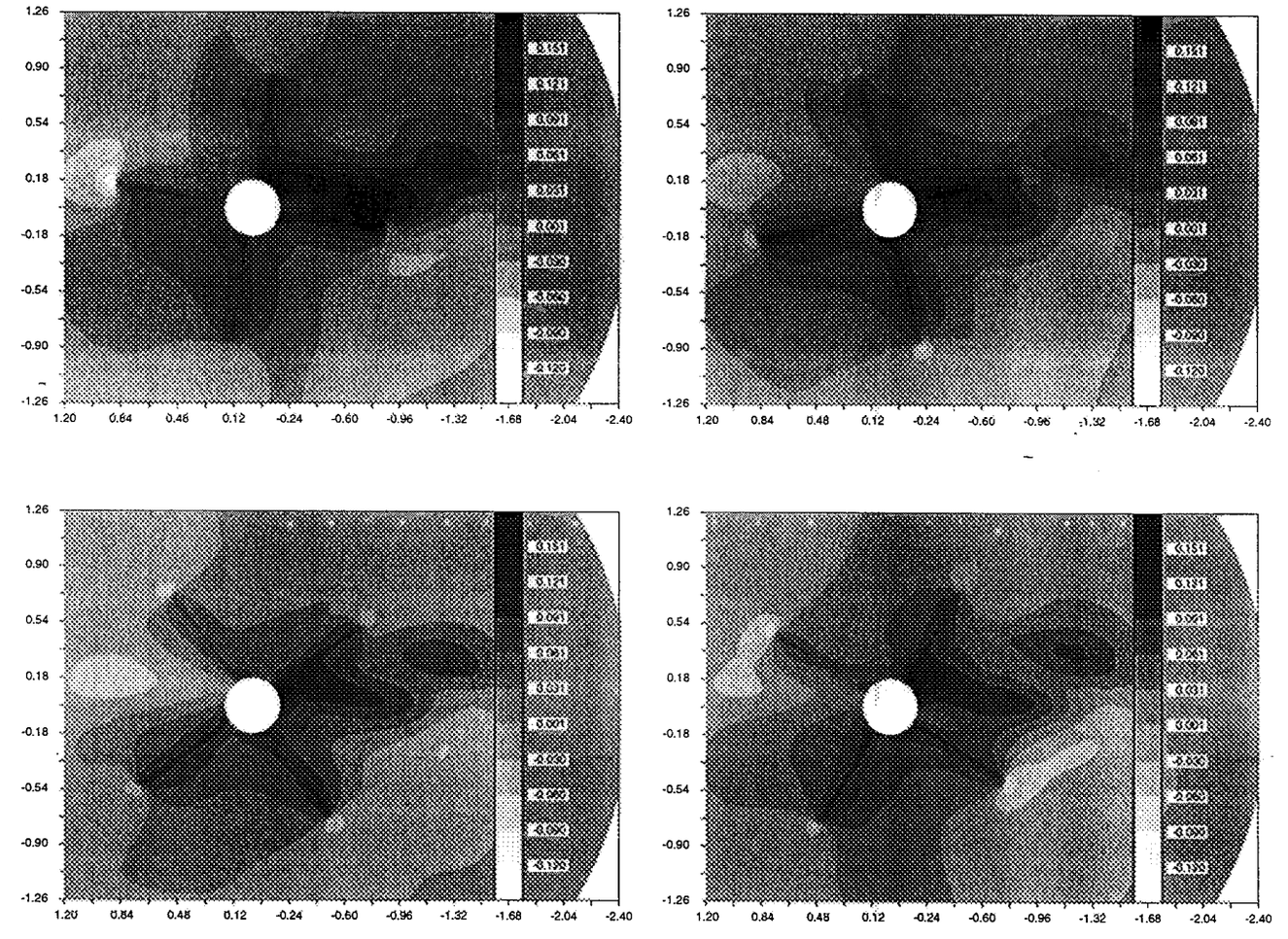

Figure 6: V_{cir} field on $x = 0.22$ grid surface at t_0(upper left), $t_{22.5}$(upper right), t_{45}(lower left), $t_{67.5}$(lower right)

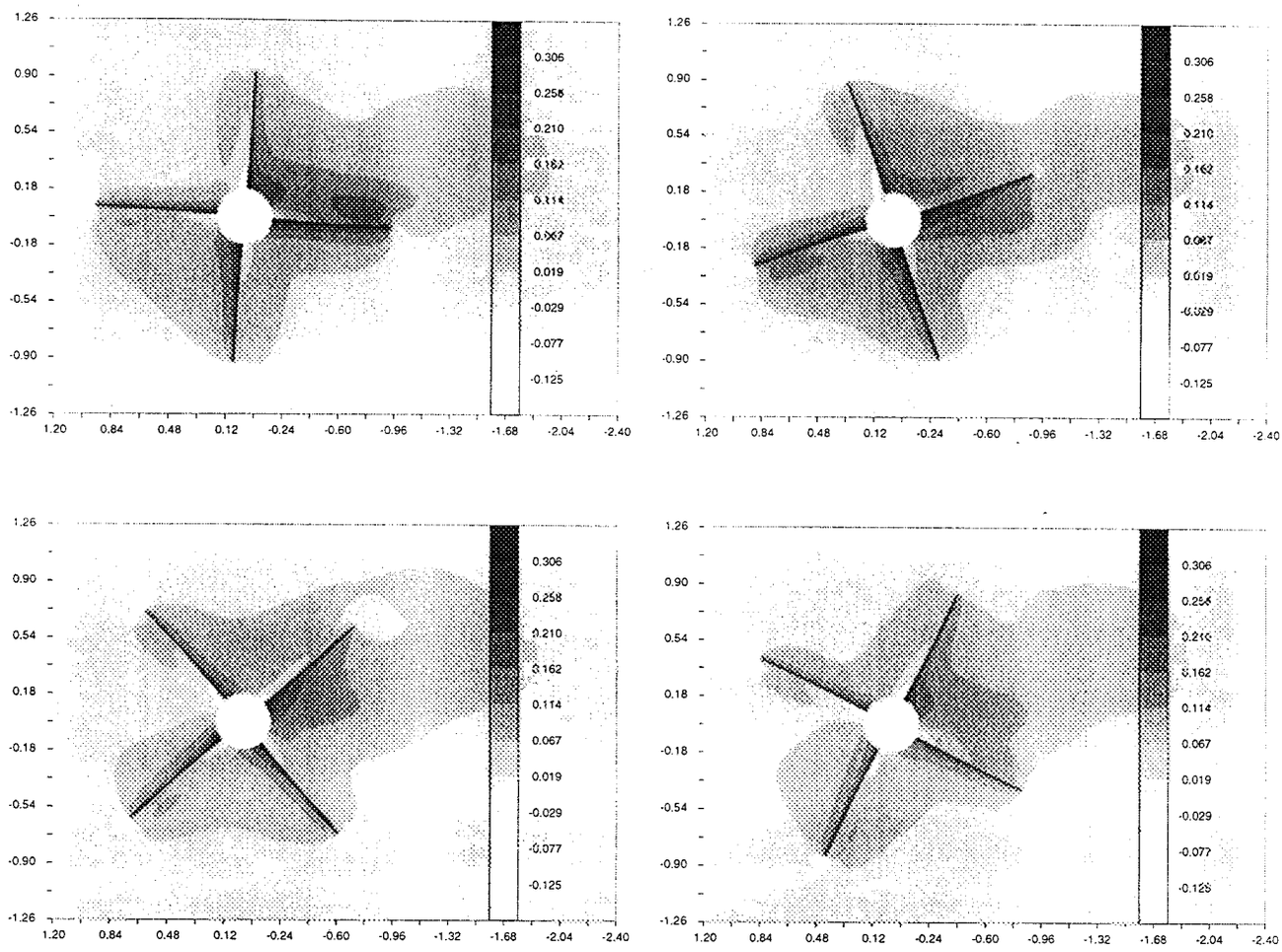

Figure 7: V_{cir} field on $x \sim 0.15$ grid surface at t_0(upper left), $t_{22.5}$(upper right), t_{45}(lower left), $t_{67.5}$(lower right)

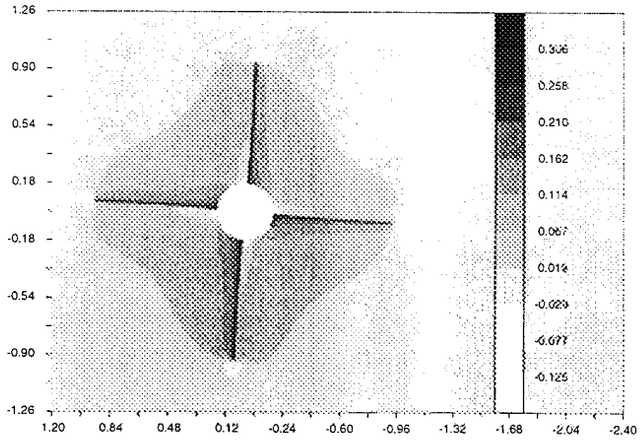

Figure 8: V_{cir} field on $x \sim 0.15$ grid surface for propeller alone at t_0

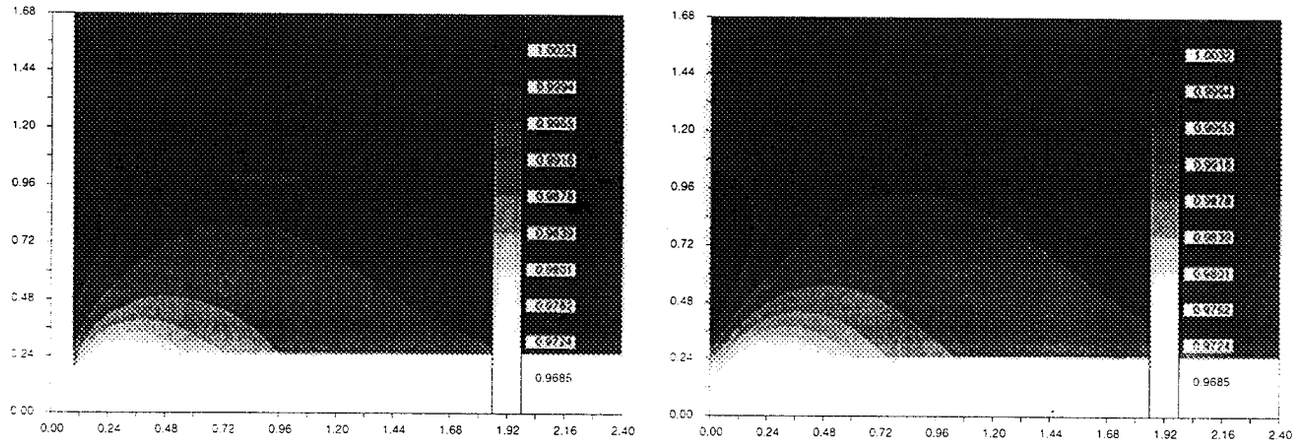

Figure 9: Comparison between the time averaged propeller results (left) and time-averaged disc model results (right): static pressure field x/r_p–r/r_p for p/p_∞

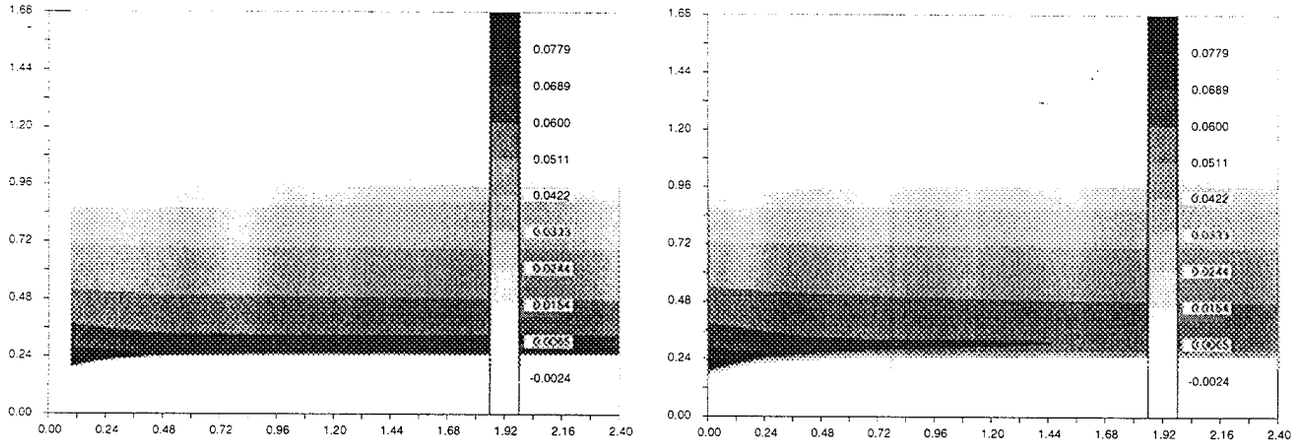

Figure 10: Comparison between the time averaged propeller results (left) and time-averaged disc model results (right): circumferential velocity field x/r_p–r/r_p for V_{cir}

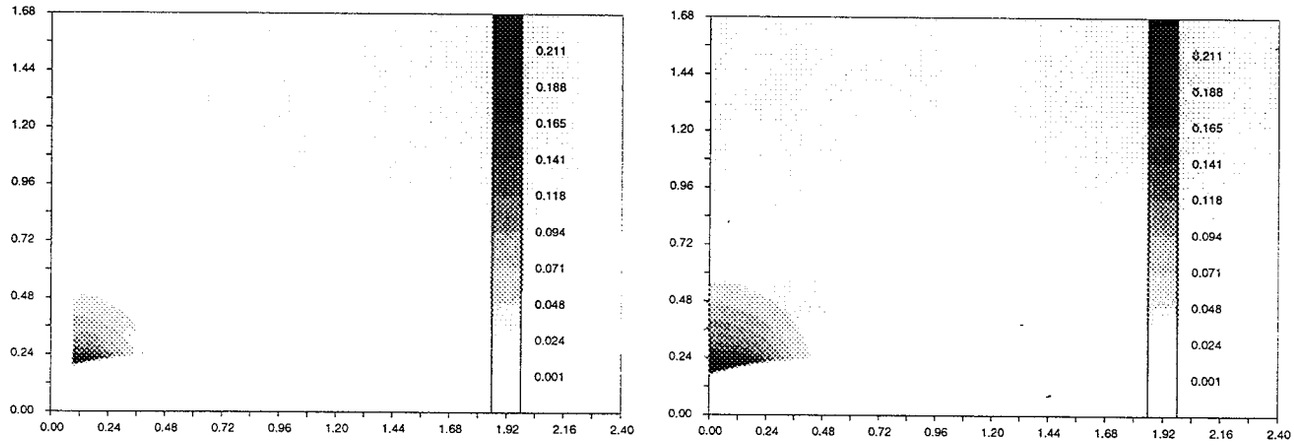

Figure 11: Comparison between the time averaged propeller results (left) and time-averaged disc model results (right): radial velocity field x/r_p–r/r_p for V_r

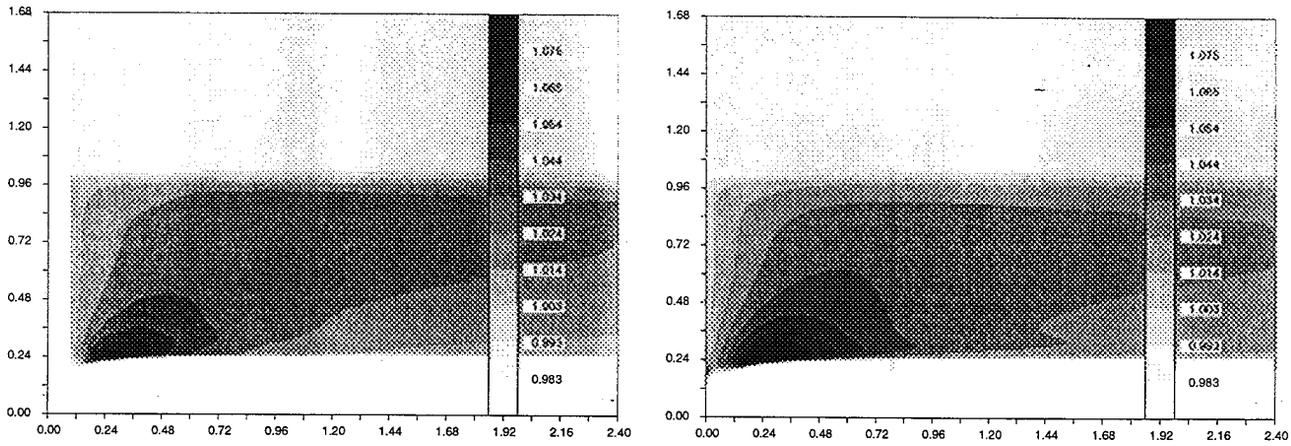

Figure 12: Comparison between the time averaged propeller results (left) and time-averaged disc model results (right): axial velocity field x/r_p–r/r_p for V_x